AIP Applied Physics Letters

Observation of quantum Talbot effect from a domain-engineered nonlinear photonic crystal

H. Jin, P. Xu, J. S. Zhao, H. Y. Leng, M. L. Zhong et al.

Citation: Appl. Phys. Lett. **101**, 211115 (2012); doi: 10.1063/1.4766728

View online: http://dx.doi.org/10.1063/1.4766728

View Table of Contents: http://apl.aip.org/resource/1/APPLAB/v101/i21

Published by the American Institute of Physics.

Observation of quantum Talbot effect from a domain-engineered nonlinear photonic crystal

H. Jin, P. Xu,[a)] J. S. Zhao, H. Y. Leng, M. L. Zhong, and S. N. Zhu
National Laboratory of Solid State Microstructures and School of Physics, Nanjing University, Nanjing 210093, China

(Received 13 September 2012; accepted 25 October 2012; published online 21 November 2012)

The quantum Talbot effect is observed from a domain-engineered nonlinear photonic crystal dispensing with a real grating. We deduce and experimentally verify the quantum self-imaging formula which is related to the crystal's structure parameter and working wavelengths. A two-photon Talbot carpet is captured to characterize the Fresnel diffraction dynamics of entangled photons wherein the quantum fractional Talbot effect is specified. The compact and stable quantum Talbot effect can be considered as the contactless diagnosis of domain's homogeneity and developed for new types of entangled photon source and quantum technologies such as quantum lithography with improved performance. © *2012 American Institute of Physics*.
[http://dx.doi.org/10.1063/1.4766728]

Talbot effect[1,2] is a well-known Fresnel diffraction phenomenon in which a periodic object illuminated with a plane wave replicates itself at multiples of a certain longitudinal propagation distance. Talbot effect holds on a variety of applications in image processing, photolithography, spectrometry, and so on.[3] It also prompts developments in the array illuminator,[4,5] hard-x-ray dark-field imaging,[6] matter waves,[7,8] and optical traps.[9] Observations of nonlinear Talbot effect[10] and plasmonic Talbot effect[11,12] are also reported, which enriches the research areas and suggests more possible applications.

Since quantum Talbot effect was conceptually proposed[13,14] and experimentally demonstrated,[15] Talbot effect has been endowed with new characters and attracts more interests. In analogy to quantum imaging, quantum Talbot effect can be nonlocal, and the Talbot length with degenerate entangled photon pairs is relevant with the pump wavelength, hence is twice of classical Talbot effect. Here we report the direct observation of quantum Talbot effect from a domain-engineered nonlinear photonic crystal (NPC). With a two-dimensional domain modulation, the NPC works as an efficient platform for entangled photon generation under quasi-phase-matching (QPM) condition; meanwhile, its transverse periodicity engenders quantum Talbot effect directly. So the quantum Talbot effect emerges dispensing with a real grating. The compact and stable quantum Talbot effect can be considered as the contactless diagnosis of domain's homogeneity and developed for new types of entangled photon source and quantum technologies such as quantum lithography with improved performance.

Domain-engineered NPCs are active in nonlinear optics for efficient frequency conversion[16] and beam shaping[17] based on the QPM technique. In quantum optics, special attentions are paid because NPCs can be utilized for the generation of bright entangled photon pairs and multifunctional manipulation of two-photon spatial entanglement.[18–20] The NPC structure in this experiment is shown in Fig. 1(a), which is a multi-stripe periodically poled lithium tantalate (MPPLT). The initial position of each stripe is precisely positioned at the same coordinate along the z axis, so that the two-photon generated from each stripe has the same initial phase. The quadratic nonlinear coefficient of the MPPLT crystal can be expressed as

$$\chi^{(2)}(x,z)=d_{33}U(x)\sum_m f(G_m)e^{iG_m z}. \quad (1)$$

The maximum nonlinear coefficient d_{33} is involved since the pump, signal, and idler are all e-polarized. $U(x)=\sum_{n=-\infty}^{\infty} rect[(x-nd)/a]$ is a grating function indicating the transverse modulation along the x-axis with period d and stripe width a. $G_m = 2\pi m/\Lambda$ is the m-th order reciprocal vector of the longitudinal domain modulation with period Λ and the corresponding Fourier coefficient is $f(G_m)$. In our experiment the first order reciprocal vector G_1 is designed for ensuring efficient generation of entangled photons under the QPM condition $k_p - k_s - k_i - G_1 = 0$.

Following the previous studies,[21,22] we trivialize the temporal part of the state and write the two-photon state as

$$|\psi\rangle = \psi_0 \int d\vec{\kappa}_s d\vec{\kappa}_i \int d\vec{\rho}\{E_p(\vec{\rho})U(\vec{\rho})\}e^{-i(\vec{\kappa}_s+\vec{\kappa}_i)\cdot\vec{\rho}} a^{\dagger}_{\vec{\kappa}_s} a^{\dagger}_{\vec{\kappa}_i}|0\rangle, \quad (2)$$

where ψ_0 is a normalization constant and $\vec{\kappa}_s$ and $\vec{\kappa}_i$ are the transverse wave vectors of signal and idler photons, respectively. For simplicity, the pump field $E_p(\vec{\rho})$ is assumed to be even distributed. Since the domain along the y-axis is homogenous, the transverse modulation function $U(\vec{\rho})$ can be written as $U(x)$ and expanded as the Fourier series $U(x)=\sum_{n=-\infty}^{\infty} c_n e^{i2\pi nx/d}$, where c_n is the Fourier coefficient of the n-th harmonic.

The two-photon spatial correlation for free propagating entangled photons can be derived as[21,22]

a)Author to whom correspondence should be addressed. Electronic mail: pingxu520@nju.edu.cn.

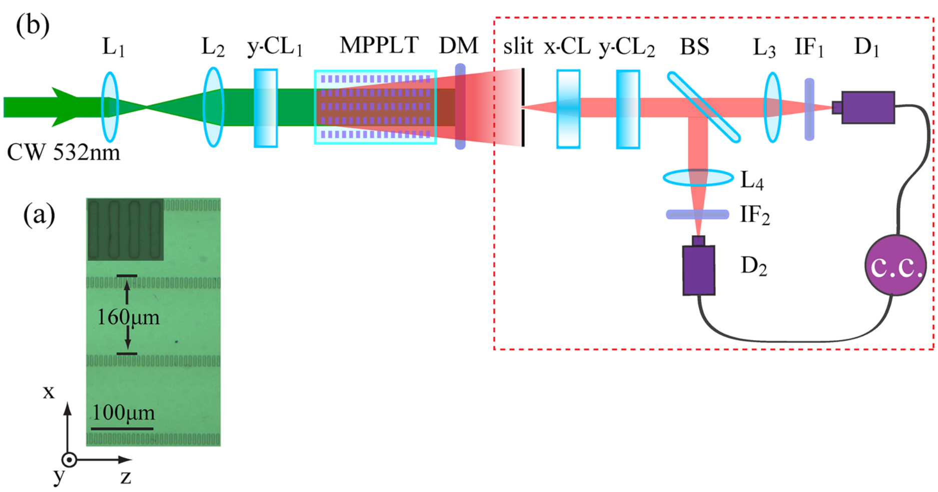

FIG. 1. (a) Micrograph of the etched MPPLT. (b) Experimental setup. L_1-L_4 are convex lenses, y-CL_1 and y-CL_2 are cylindrical lenses focusing along the y-axis, and x-CL is a cylindrical lens focusing along the x-axis.

$$R_{c.c.}(x_s, z_s; x_i, z_i) \propto |\langle 0|E_1^{(+)}E_2^{(+)}|\psi\rangle|^2 \propto \left|\int dx_0 e^{i\pi\eta(x_0-\xi)^2}U(x_0)\right|^2$$
$$\propto \left|\sum_{n=-\infty}^{\infty} c_n e^{i2\pi n\xi/d} e^{-i\pi n^2/(d^2\eta)}\right|^2, \tag{3}$$

where $\eta = 1/(\lambda_s z_s) + 1/(\lambda_i z_i)$, $\xi = \left(\frac{x_s}{\lambda_s z_s} + \frac{x_i}{\lambda_i z_i}\right)/\left(\frac{1}{\lambda_s z_s} + \frac{1}{\lambda_i z_i}\right)$, $E_1^{(+)}$ and $E_2^{(+)}$ are the electric fields evaluated at the two detectors, λ_s and λ_i are the wavelengths of signal and idler photons, respectively, z_s (z_i) is the distance from the crystal to the plane where the single photon detector D_1 (D_2) lies in, x_0 is the transverse coordinate of the output plane of the crystal, and x_s (x_i) is the detector's transverse coordinate. The first exponential term in Eq. (3) is the n-th Fourier component of a periodic function, and the second one is a phase shift dependent on the order of the Fourier component. If the second term equals 1 for all n, that is

$$\frac{1}{\lambda_s z_s} + \frac{1}{\lambda_i z_i} = \frac{1}{2md^2}, \tag{4}$$

where m is an integer indicating the m-th Talbot plane, Eq. (3) turns into a reproduction of grating function. So the quantum Talbot effect is directly observable after the MPPLT crystal. Since ξ is an associate coordinate, the Talbot self-image of the domain structure is magnified, and the exhibited period depends on the way of detection and the wavelengths of the photon pair. In particular, when we set $z_s = z_i = z$ and $x_s = x_i = x$ which is an in-step measurement, Eq. (3) indicates the two-photon amplitude can be equivalently considered as the pump photon's Fresnel diffraction, and the coincidence counting rate exactly replicates the transverse domain function, i.e., $R_{c.c.} \propto U(x)$ at the Talbot plane $z_T = 2d^2/\lambda_p$ and multiples of that. So the two-photon Talbot length is defined by the wavelength of pump wave, which is different from the classical one.

Fig.1(a) shows the micrograph of the ferroelectric domain structure of the etched MPPLT sample used in this experiment. The longitudinal periodicity is $\Lambda = 7.548\,\mu$m for all stripes, which contributes to the QPM condition during the generation of entangled photons when the sample works at 170 °C. The transverse stripe interval is $d = 160\,\mu$m with stripe width $a = 20\,\mu$m and stripe length $L = 10$ mm. The two-photon Talbot length is $z_T = 96.2$ mm when the crystal is pumped by 532 nm.

Experimentally the two-photon Talbot effect is studied under two schemes. In the first one, both detectors are placed at the same distance from the output face of the crystal and scan in step along the same direction. As sketched in Fig. 1(b), in order to produce the degenerate photon pairs at 1064 nm, the crystal is pumped with a CW single longitudinal mode 532 nm laser. The pump is first expanded and collimated by two convex lenses L_1 and L_2 and focused along the y-axis by a cylindrical lens y-CL_1. After the crystal, the entangled photons are first separated from the pump by a dichromatic mirror DM. A 20 μm slit is used to scan along the x-axis and cascaded by a two-photon coincidence counting measurement. Specifically, after the slit, the entangled photons are collimated by two cylindrical lenses x-CL and y-CL_2, separated by a beam splitter and finally collected into two single photon detectors D_1 and D_2, respectively, by two collection lenses. Preceding each detector is a 10 nm bandwidth interference filter centered at 1064 nm to further suppress the pump. The slit and cascaded x-CL are fixed on a motorized precision positioning stage which can scan in both x and z directions. The slit and the following components can be regarded as an assembly two-photon detector denoted by a dashed rectangle in Fig. 1(b), which is capturing two-photon probability at the slit position.

In Fig. 2(a) we show the coincidence counts between two detectors as well as the D_1 single counts versus the transverse position of the slit when located at the first Talbot length $z_T = 96.2$ mm. The single counting rate shows an even distribution, whereas the coincidence counting rate reveals a periodic interference pattern with the periodicity of 160 μm, which is just the same as the transverse separation d of domain stripes; thus, the two-photon Talbot effect is confirmed. The fitted value for the full width at $1/e^2$ of the maximum of each correlation peak is $33.9 \pm 1.8\,\mu$m which is larger than the theoretical value 24.1 μm due to that the spatial resolution is limited by the 20 μm scanning slit. The theoretical value is given under the 5 mm pump beam size ($1/e^2$), and the Fresnel diffraction broadens the image of each stripe. In order to investigate the two-photon diffraction dynamics, we capture a two-photon Talbot carpet as shown in Fig. 2(b) by measuring two-photon correlation in different detection planes located from $(1/2)z_T$ (48.1 mm) to $(3/2)z_T$ (144.3 mm) by the step size of 1 mm. The measured two-photon Talbot carpet is in good agreement with the theoretical one as

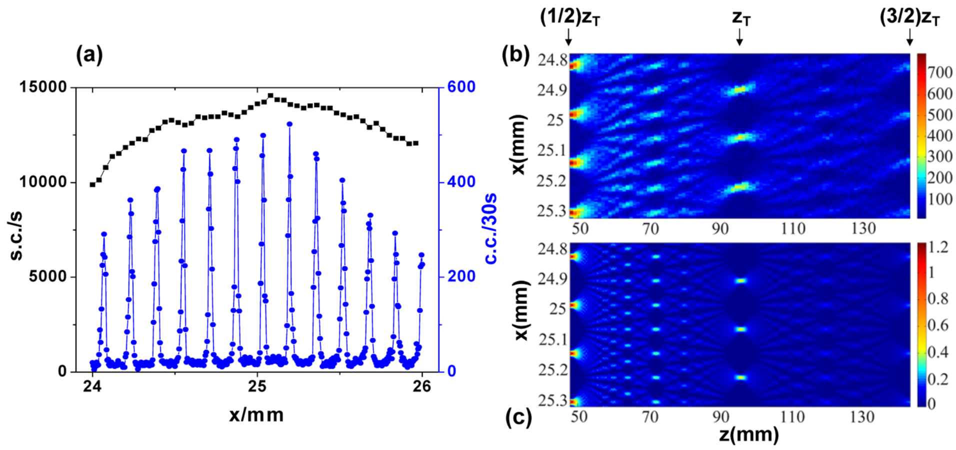

FIG. 2. (a) Measured single counts (black squares) and coincidence counts (blue dots) versus the transverse position of the slit at the first Talbot length $z_T = 96.2$ mm. (b) Experimental and (c) theoretical two-photon Talbot carpet from $(1/2)z_T$ (48.1 mm) to $(3/2)z_T$ (144.3 mm).

shown in Fig. 2(c). From the two-photon Talbot carpet, it is convenient for understanding the evolution of the two-photon diffraction and interference when the photon pair propagates in the free space. At distances $(1/2)z_T$ and $(3/2)z_T$, the two-photon interference patterns are the same as that at z_T except with a half-period shift. Besides these integer Talbot images, fractional images[7,23] with a reduced period $(1/n)d$ ($n = 2,3,4$) are picked out and shown in Figs. 3(b)–3(d).The integer images at z_T and $(1/2)z_T$ are also shown for comparison in Figs. 3(a) and 3(e), respectively. For quantum Talbot imaging, there is no net improvement in the spatial resolution[15] due to the doubled Talbot length, which is different from quantum lithography.

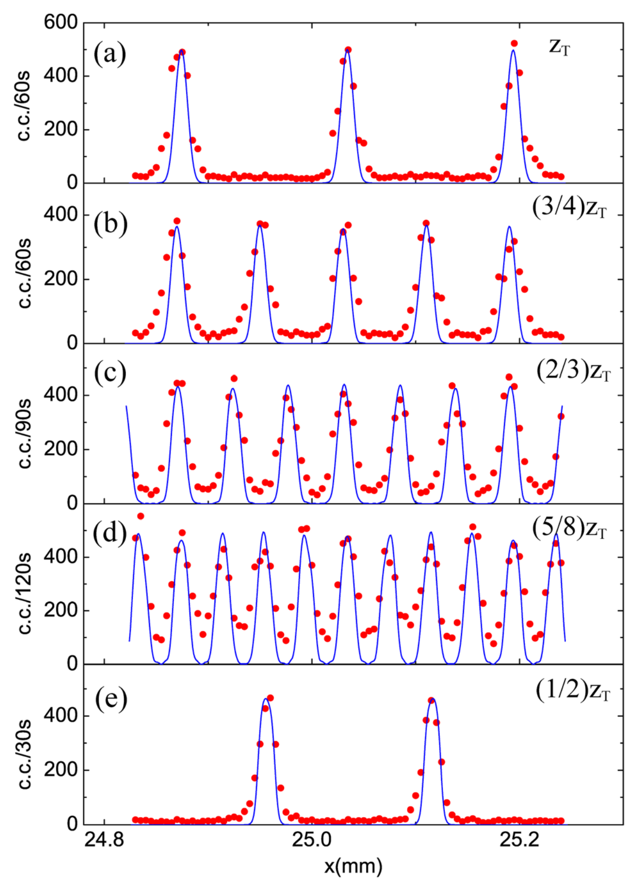

FIG. 3. The red dots are the measured integer two-photon Talbot images detected at distances of (a) z_T, (e) $(1/2)z_T$ and fractional images at distances of (b) $(3/4)z_T$, (c) $(2/3)z_T$, and (d) $(5/8)z_T$. The blue lines are theoretical curves.

In order to verify the self-imaging condition $\frac{1}{z_s} + \frac{1}{z_i} = \frac{2}{z_T}$ for degenerate photon pairs indicated by Eq. (4) and disclose the physics of Talbot effect more intuitively, we carry out the two-photon Talbot experiment with another scheme. In this scheme, the two detectors scan independently. As shown in Fig. 4(a), the entangled photon pairs are separated by a 50/50 beam splitter. For each path, the single photon collection scheme is similar with Fig. 1(b), a 20 μm slit cascaded by two cylindrical lens x-CL_1 (x-CL_2) and y-CL_2 (y-CL_3) scans to give the coincidence counts. The slit and the following components can be regarded as an assembly detector D_1 (D_2) whose detection position is determined by the position of the slit. When both detectors are located at z_T, the coincidence counts still presents a grating function as shown in Fig. 4(e) except that the period is $2d$, which is twice of the transverse period of the MPPLT sample. Then we fix the detector D_2 at $z_T \pm 5$ mm and $z_T \pm 10$ mm, respectively, and perform a two-dimensional scanning of D_1 along the x and z directions to find out the corresponding self-imaging distances as shown in the inset in Fig. 4(b), where the values of coincidence counts are represented by brightness. Fig. 4(b) shows the measured self-imaging formula by five sets of z_s and z_i which consists well with Eq. (4). When the detector D_2 is fixed at distances $z_i = z_T - 10$ mm, $z_i = z_T - 5$ mm, $z_i = z_T + 5$ mm, $z_i = z_T + 10$ mm, the self-images are shown in Figs. 4(c), 4(d), 4(f), and 4(g), respectively. The coincidence counts exhibit images with the magnification of $1 + \frac{z_s}{z_i}$, which can be derived from Eq. (3). This experiment further differs the Talbot self-imaging from the conventional imaging by a lens. A point to point correspondence between the image plane and object plane is established by a lens, which means that in the imaging process, every point on the object corresponds to only one point, or spot more precisely due to the diffraction effect, on the image plane. However, in the experiment above, the coincidence counts show one-to-many relationship, which intuitively discloses that Talbot self-image is not a real image but a result of optical interference. Quantum Talbot image supplies more insights on the physics of Talbot effect.

It is worth noting that for the direct quantum Talbot imaging after the MPPLT, since the entangled photon pair can be designed at any wavelength within the transmitted window of the material due to the versatility of QPM, two-color Talbot effect is expected to be achieved easily. Furthermore, when implementing the two-color Talbot effect by scanning the two

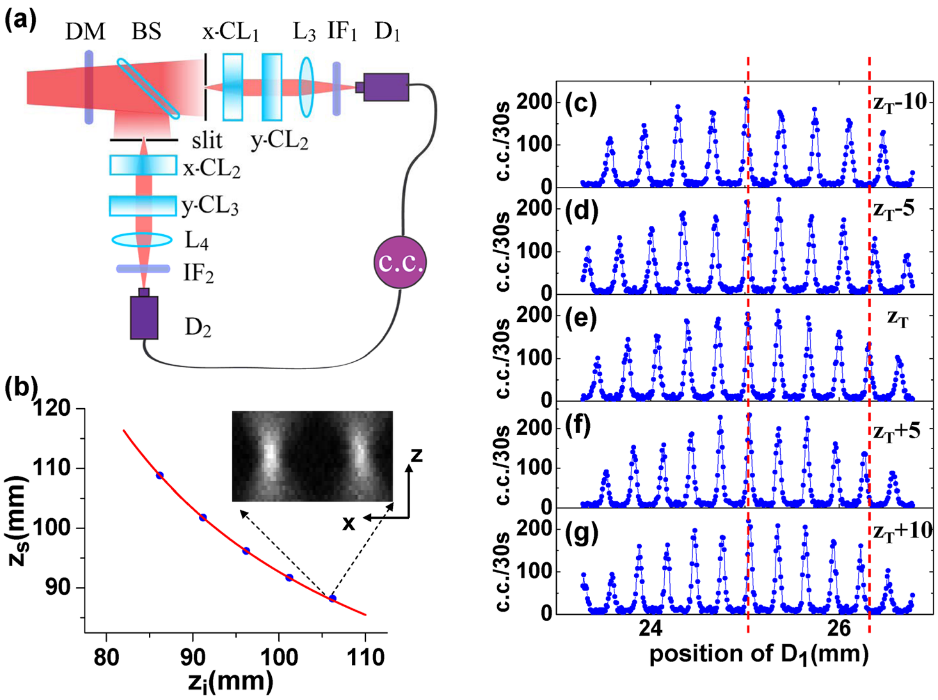

FIG. 4. (a) The experimental setup of the detection part for the second scheme. (b) The relationship between two detection distances when Talbot images occur. The blue dots are measured results and the red line is a theoretical curve. The inset shows the measured coincidence counts as detector D_1 scans at different distances while D_2 is fixed at $z_T + 10$ mm. (c)-(g) The measured coincidence counts versus the transverse position of detector D_1 when D_2 is fixed at distances of (c) $z_i = z_T - 10$ mm, (d) $z_i = z_T - 5$ mm, (e) $z_i = z_T$, (f) $z_i = z_T + 5$ mm, and (g) $z_i = z_T + 10$ mm.

detectors in step but in opposite direction, two-photon interference at the Talbot plane z_T will exhibit the beating pattern with a magnified period $\frac{\lambda_s+\lambda_i}{\lambda_s-\lambda_i}d$. The Talbot beating effect may be employed as an effective way to reveal the periodic domain with an extremely small separation.

In conclusion, from a two-dimensional domain engineered lithium tantalate, we observed the direct quantum Talbot effect. With no real grating involved, the direct quantum Talbot effect results from the periodicity of two-photon spatial mode, hence is an inherent phenomenon existing concomitantly within the spontaneous parametric down conversion for entangled photons. By examining the propagation dynamics of two-photon diffraction and interference within one Talbot length, we capture the two-photon Talbot carpet and verify the self-imaging condition. With entangled photon pairs, it is more intuitive to reveal the hypostasis of Talbot effect as a diffraction phenomenon instead of imaging. Since the absence of grating and lens can improve stability and miniaturization, our results may be helpful for developing new types of entangled photon source and quantum technologies such as quantum lithography with improved performance when the flexible QPM technique is involved.

The authors thank L. A. Wu and J. M. Wen for valuable discussions. This work was supported by the State Key Program for Basic Research of China (Nos. 2012CB921802 and 2011CBA00205), the National Natural Science Foundations of China (Nos. 11174121, 91121001, and 11021403), the Project Funded by the Priority Academic Program Development of Jiangsu Higher Education Institutions (PAPD), and a Foundation for the Author of National Excellent Doctoral Dissertation of PR China (FANEDD).

[1]H. F. Talbot, Philos. Mag. **9**, 401 (1836).
[2]L. Rayleigh, Philos. Mag. **11**, 196 (1881).
[3]K. Patorski, in *Progress in Optics*, edited by E. Wolf (North-Holland, Amsterdam, 1989), Vol. 27, pp. 1–108.
[4]A. W. Lohmann and J. A. Thomas, Appl. Opt. **29**, 4337 (1990).
[5]P. Maddaloni, M. Paturzo, P. Ferraro, P. Malara, P. De Natale, M. Gioffrè, G. Coppola, and M. Iodice, Appl. Phys. Lett. **94**, 121105 (2009).
[6]F. Pfeiffer, M. Bech, O. Bunk, P. Kraft, E. F. Eikenberry, C. H. Brönnimann, C. Grünzweig, and C. David, Nat. Mater. **7**, 134 (2008).
[7]S. Nowak, Ch. Kurtsiefer, T. Pfau, and C. David, Opt. Lett. **22**, 1430 (1997).
[8]B. Brezger, L. Hackermüller, S. Uttenthaler, J. Petschinka, M. Arndt, and A. Zeilinger, Phys. Rev. Lett. **88**, 100404 (2002).
[9]Y. Y. Sun, X.-C. Yuan, L. S. Ong, J. Bu, S. W. Zhu, and R. Liu, Appl. Phys. Lett. **90**, 031107 (2007).
[10]Y. Zhang, J. M. Wen, S. N. Zhu, and M. Xiao, Phys. Rev. Lett. **104**, 183901 (2010).
[11]M. R. Dennis, N. I. Zheludev, and F. J. García de Abajo, Opt. Express **15**, 9692 (2007).
[12]D. van Oosten, M. Spasenovic, and L. Kuipers, Nano Lett. **10**, 286 (2010).
[13]K. H. Luo, J. M. Wen, X. H. Chen, Q. Liu, M. Xiao, and L. A. Wu, Phys. Rev. A **80**, 043820 (2009); **83**, 029902(E) (2011).
[14]C. H. R. Ooi and B. L. Lan, Phys. Rev. A **81**, 063832 (2010).
[15]X. B. Song, H. B. Wang, J. Xiong, K. G. Wang, X. D. Zhang, K. H. Luo, and L. A. Wu, Phys. Rev. Lett. **107**, 033902 (2011).
[16]M. M. Fejer, G. A. Magel, D. H. Jundt, and R. L. Byer, IEEE J. Quantum Electron. **28**, 2631 (1992).
[17]J. R. Kurz, A. M. Schober, D. S. Hum, A. J. Saltzman, and M. M. Fejer, IEEE J. Sel. Top. Quantum Electron. **8**, 660 (2002).
[18]J. P. Torres, A. Alexandrescu, S. Carrasco, and L. Torner, Opt. Lett. **29**, 376 (2004).
[19]X. Q. Yu, P. Xu, Z. D. Xie, J. F. Wang, H. Y. Leng, J. S. Zhao, S. N. Zhu, and N. B. Ming, Phys. Rev. Lett. **101**, 233601 (2008).
[20]H. Y. Leng, X. Q. Yu, Y. X. Gong, P. Xu, Z. D. Xie, H. Jin, C. Zhang, and S. N. Zhu, Nat. Commun. **2**, 429 (2011).
[21]M. H. Rubin, Phys. Rev. A **54**, 5349 (1996).
[22]P. Xu, H. Y. Leng, Z. H. Zhu, Y. F. Bai, H. Jin, Y. X. Gong, X. Q. Yu, Z. D. Xie, S. Y. Mu, and S. N. Zhu, Phys. Rev. A **86**, 013805 (2012).
[23]Z. H. Chen, D. M. Liu, Y. Zhang, J. M. Wen, S. N. Zhu, and M. Xiao, Opt. Lett. **37**, 689 (2012).